






Original Article


Alpine vegetation responses to snow phenology in the Chinese Tianshan mountainous region

ZHANG Bo^{1,2,3}  <https://orcid.org/0000-0002-2578-365X>; e-mail: 18235118550@163.com

LI Xue-mei^{1,2,3*}  <https://orcid.org/0000-0002-9630-2673>;  e-mail: lixuemei@lzjtu.edu.cn

LI Chao⁴  <https://orcid.org/0000-0002-7486-7884>; e-mail: 0218732@stu.lzjtu.edu.cn

NYIRANSENGIYUMVA Christine^{1,2,3}  <https://orcid.org/0000-0003-3096-7696>; e-mail: qrystine1@gmail.com

QIN Qi-yong^{1,2,3}  <https://orcid.org/0000-0001-7424-5084>; e-mail: qinqiyong2021@163.com

*Corresponding author

¹ Faculty of Geomatics, Lanzhou Jiaotong University, Lanzhou 730070, China

² Gansu Provincial Engineering Laboratory for National Geographic State Monitoring, Lanzhou 730070, China

³ National-Local Joint Engineering Research Center of Technologies and Applications for National Geographic State Monitoring, Lanzhou 730070, China

⁴ College of Urban and Environmental Science, Northwest University, Xian 710127, China

Citation: Zhang B, Li XM, Li C, et al. (2022) Alpine vegetation responses to snow phenology in the Chinese Tianshan mountainous region. *Journal of Mountain Science* 19(5). <https://doi.org/10.1007/s11629-021-7133-4>

© Science Press, Institute of Mountain Hazards and Environment, CAS and Springer-Verlag GmbH Germany, part of Springer Nature 2022

Abstract: Investigating the interrelation between snow and vegetation is essential to explain the response of alpine ecosystems to climate change. Based on the MOD10A1 daily cloud-free snow product and MOD13A1 NDVI (normalized difference vegetation index) data, this study analysed the spatial and temporal patterns of snow phenology including snow onset date, snow end date, snow cover days, and vegetation phenology including the start of growing season, the end of growing season and the length of growing season in the Chinese Tianshan Mountainous Region (CTMR) from 2002 to 2018, and then investigated the snow phenological effects on the vegetation phenology among different ecogeographic zones and diverse vegetation types. The results indicated that snow onset date was earlier at higher elevations and later at lower elevations, while snow end date showed opposite spatial distribution

characteristics. The end of growing season occurred later on the northwest slope of the CTMR and the Yili Valley. The earliest end of growing season was in the middle part of the CTMR. A long growing season was mainly distributed along the northern slope and the Yili Valley, while a short growing season was concentrated in the middle part of the CTMR. The response of vegetation phenology to changes in snow phenology varied among vegetation types and ecogeographic zones. The effect of snow phenology on vegetation phenology was more significant in IID5 (Yili Valley) than in the other ecogeographic zones. A negative correlation was observed between the start of growing season and snow end date in nearly 54.78% of the study area, while a positive correlation was observed between the start of growing season and the snow end date in 66.85% of the study area. The sensitivity of vegetation phenology to changes in snow cover varied among different vegetation types. Snow onset date had the greatest effect on the start of growing season in the four vegetation cover types (alpine meadows, alpine steppes, shrubs, and alpine

Received: 18-Oct-2021

1st Revision: 13-Jan-2022

2nd Revision: 16-Mar-2022

Accepted: 29-Mar-2022

sparse vegetation), whereas the snow cover days had the least impact. Snow end date had the greatest impact on the end of growing season in the alpine steppes and shrub areas. The study results are helpful for understanding the vegetation dynamics under ongoing climate change, and can benefit vegetation management and pasture development in the CTMR.

Keywords: Snow phenology; Vegetation phenology; Climate change; Response mechanism; Grey correlation analysis; Chinese Tianshan Mountainous Region

1 Introduction

Alpine vegetation plays an indispensable role in the water resources, seasonal carbon, and energy cycle (Körner 2005; Miao et al. 2015). Many aspects of alpine vegetation can be affected by climate, such as vegetation composition, productivity, multiplicity, phenology and vegetation fraction (Ozanne et al. 2003; Zhang et al. 2010; Thomey et al. 2011; Thompson et al. 2015; Wu et al. 2016; Liu et al. 2017). As an essential climate driving factor, snow phenology can directly or indirectly reflect the climate, hydrology and ecological conditions of a region (Thackeray et al. 2016; Wang et al. 2016), and it has an important effect on the global energy balance and the circulation of water resource (Ahmed et al. 2020). Thus, accounting for snow phenology is important for meteorological predictions, climate research, hydrological processes, ecological civilization and social production (Chen et al. 2015a; Chen et al. 2015b). In recent years, many experiments and observations have shown that the phenological change of vegetation phenology is closely related to seasonal snow cover. (Thompson et al. 2015; Jin et al. 2017). The change of winter snow cover also influenced vegetation growth and productivity (Sa et al. 2021). The study on the response of alpine vegetation to global warming helps to reveal the impacts of snow cover change on alpine ecosystem under global warming.

Changes in snow can alter energy flows and water circulation patterns, which were essential for the growth of vegetation (Buus et al. 2006). Snow not only stores soil moisture, regulates alpine vegetation growth, blocks sunlight needed for photosynthesis and ensures plant growth and development but also protects vegetation from the destruction caused by

dry and cold climatic conditions. Moreover, it also provides a certain amount of water vapour for vegetation (Inouye et al. 2008; Ide et al. 2013; Desai et al. 2015; Xie et al. 2017; Frick et al. 2019). Since the soil thawing time and subsequent soil water content are the main factors affecting the phenology of vegetation in temperate and cold zones, snow phenology may affect the seasonality of terrestrial systems by changing the date of soil freezing and thawing (Shen et al. 2011). A previous study demonstrated that snow phenology is vital for vegetation phenology in snowy and dry areas (Paudel et al. 2013). Climate warming and snow meltwater accelerated the vegetation growth after long and cold winters (Dorji et al. 2013). Some scholars have described the interrelation between vegetation phenology and snow cover so far. Julitta et al. (2014) suggested that the snowmelt date was negatively correlated with the start date of the growing season. Vitase et al. (2017) identified a strong relationship between spring snowmelt time and vegetation growing season initiation date in environments with long snow cover, and they found that spring snowmelt time was the best predictor of vegetation growing season initiation. Over the past three decades, the Qinghai-Tibet Plateau has experienced a significant warming trend. The snow cover in the region has also changed significantly, which may affect the trend of the spring runoff and surface phenology (Wang et al. 2013). The research conducted by Wang et al. (2017) elucidated the vegetation phenology response to dynamics in snow phenology on the alpine ecosystem in the Tibetan Plateau, which suggested that the response of vegetation to snow varies for different vegetation types. Wang concluded that the responses of vegetation phenology to snow dynamics were diverse under different climate conditions, topographic conditions and alpine vegetation communities (Wang et al. 2015).

The Chinese Tianshan mountainous region (CTMR) is an alpine region with unique topographic and climatic conditions, and it presents abundant precipitation, snow-capped peaks year round, and abundant snow resources. The topography of the CTMR is complex, with some parts (the northern slopes of the CTMR) showing a distinct vertical structural distribution of vegetation. Over the past three decades, the CTMR has experienced a significant warming trend (Li et al. 2016), which has led to significant changes in snow cover. The warming

resulted in earlier snowmelt dates, which may further alter the flow and time of spring snowmelt runoff and increase the risk of spring floods and summer droughts (Chen et al. 2015). Alpine vegetation is essential for ecosystem carbon cycling and water cycling (Richardson et al. 2013), and it has diverse roles, such as conserving water sources, regulating climate and providing animal and microbial habitats (Wang et al. 2013). The change in snow phenology is caused by differences in the climate, hydrography and ecological environment in this region, and it has a controlling impact on the beginning and length of the vegetation growing season. However, research on the impact of snow cover on alpine vegetation phenology at home and abroad is still scarce and unsystematic. In particular, the response of alpine vegetation phenology to dynamic changes in snow cover in the CTMR has rarely been studied. Therefore, it is urgent to conduct in-depth research on the response of alpine vegetation phenology to snow dynamics in the CTMR under the background of rapid climate warming.

In this paper, the start of growing season (SOS), the end of growing season (EOS) and the length of growing season (LOS) were calculated as indicators of vegetation growth dynamics. Moreover, snow cover days (SCD), snow onset date (SOD) and snow end date (SED) were extracted based on cloud-free snow products. Then, we analysed the response of vegetation phenology to changes in snow phenology in different ecogeographic zones and with different vegetation cover types. The objectives of this study were to (1) investigate the spatiotemporal variation in snow phenology and alpine vegetation phenology in the CTMR under the background of rapid climate warming and (2) reveal the response relationship between alpine vegetation phenology and snow phenology in the CTMR.

2 Study Area

The CTMR stretches across central Xinjiang and has a total length of 1700 km and an average ridge height of 4000 m asl, and it is the climatic watershed of northern and southern Xinjiang (Hu et al. 2004; Li et al. 2018). The region is dominated by a typical temperate continental arid and semiarid climate, which is characterized by temperature extremes in summer and winter (Li et al. 2020). The CTMR is

located in the inland midlatitude westerly zone. The water vapour mainly comes from the west and northwest, and the precipitation is greatly influenced by the north and south jet streams. In winter, under the control of high pressure, the weather is stable, and the climate is cold. In spring, the north ramus jet stream is active north of the CTMR, and precipitation increases. In summer, the surface cyclones generated by the disturbance of the southern ramus jet invade from the southwest and form strong rain and snow weather in the CTMR. In autumn, the CTMR is under the control of rapidly increasing high pressure and presents crisp weather (Zhang et al. 1987). Most of the precipitation falls on the windward west and northwest slopes, which are affected by cold northerly and northwesterly air currents, and by westerly humid air currents from the North Atlantic (Liu et al. 2017). The CTMR has the particular characteristics because of its unique geographical conditions. The CTMR has unique climatic conditions and presents a typical alpine vegetation ecosystem that includes desert (30.5%), alpine steppes (26.6%), alpine meadows (18.3%), sparse alpine vegetation (8.7%), forest (3.8%), shrub (0.7%), cushion vegetation (0.9%), no vegetation (6.8%), arable land (3.4%), permanent wetland (0.3%), and water (0.1%) (Fig. 1a). Since more than 54% of the alpine vegetated area in the CTMR consists of alpine steppes, alpine meadows, alpine sparse vegetation, and shrubs, we mainly selected these four vegetation types. Based on the objectives of this study, the mutual response relationships between vegetation phenology and snow phenology were assessed. This paper divided the CTMR into four ecogeographic zones based on the eco-geographical characteristics (Table 1, Fig. 1).

3 Data and Methods

3.1 Datasets

Snow data were obtained from the 2002-2018 daily cloud-free snow cover dataset for High Asia provided by the National Glacial Permafrost and Desert Data Centre (Qiu et al. 2020). The spatial resolution was 500 m, and verification with field observations indicated 85.79% agreement. The mean absolute error between the snow cover days (SCD) extracted from Moderate-Resolution Imaging Spectroradiometer (MODIS) data and the measured

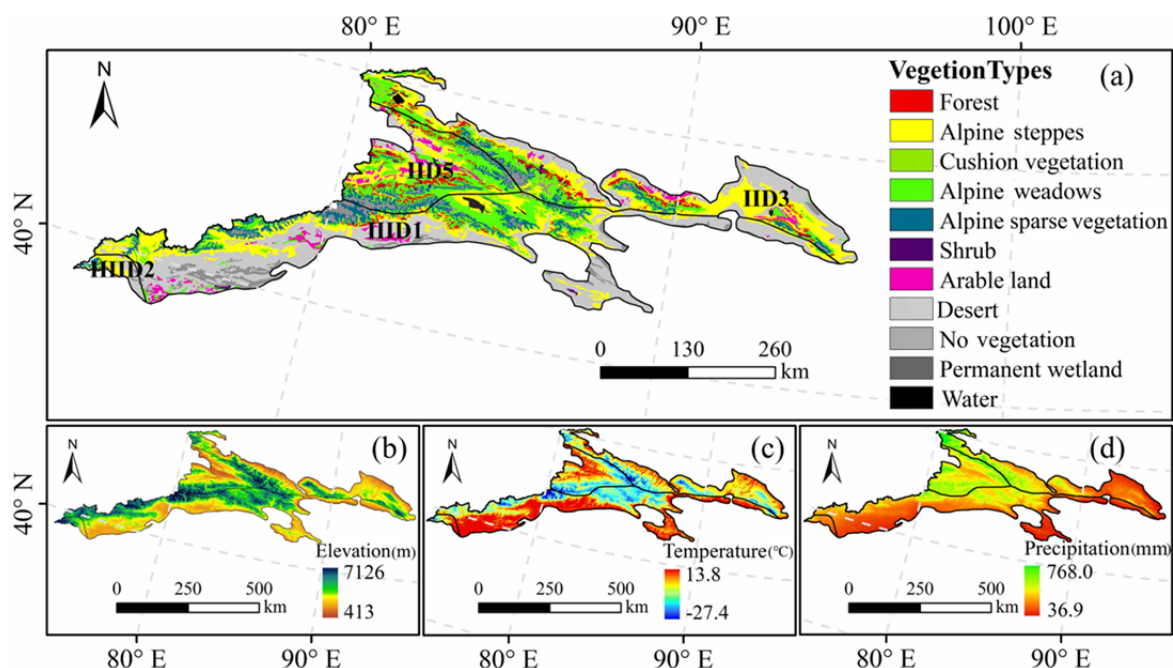


Fig. 1 Description of the vegetation types and ecogeographical zones (a), elevation (b), annual mean temperature (c), and annual total precipitation (d) in the Chinese Tianshan mountainous region (CTMR).

Table 1 Ecogeographical zones in the Chinese Tianshan mountainous region

Code	Temperature zone	Humidity region	Code	Eco-geographical zone
II	Middle temperature zone	Arid zone	IID3	Junggar Basin
		Arid zone	IID5	Yili Valley
III	Warm temperature zone	Arid zone	IIID1	Tarim and Turpan Basin
HII	Plateau temperature zone	Arid zone	HIID2	Kunlun Mountain North Wing

SCD was 4.17 days (Tang et al. 2017), which ensures that the snow product can be used to monitor snow phenology.

MODIS normalized difference vegetation index (NDVI) data were obtained from the MOD13A1 product provided by the Atmosphere Archive Distribution System Distributed Active Archive Center. The spatial resolution is 500 m. The temporal resolution is 16 d. MOD13A1 was produced based on a series of complex algorithms and rigorous quality control (Justice et al. 1998). In this study, it was used to calculate the vegetation phenology parameters from 2002-2018 across the CTMR.

The meteorological data were based on the monthly 1 km resolution mean temperature dataset (Peng et al. 2017; Peng et al. 2018; Peng et al. 2019; Peng et al. 2019; Ding et al. 2020) and monthly precipitation dataset (Peng et al. 2017; Peng et al. 2018; Peng et al. 2019; Ding et al. 2020; Peng et al. 2020) provided by the National Qinghai-Tibet Plateau Scientific Data Centre. Among them, the units of monthly average temperature and precipitation data

are 0.1°C and 0.1 mm, respectively.

Digital elevation model (DEM) data were obtained from the Scientific Data Centre of Cold and Arid Regions of the Chinese Academy of Sciences. Vegetation type data (Chinese 1:1 million vegetation type data) were from the Resource and Environmental Science Data Centre of the Chinese Academy of Sciences. In this study, according to the three dimensions of plant classification data, topographic characteristics and vegetation cover types in the study area were divided into four types, namely, alpine meadows, alpine steppes, shrubs, and alpine sparse vegetation.

3.2 Methods

3.2.1 Calculation of snow phenology

Based on the daily cloud-free snow cover products, the snow phenology parameters were calculated for each hydrological year (September 1 to August 31 of the following year) on an image-by-image basis according to the following algorithm

(Wang et al. 2009):

$$SCD = \sum_0^n H(D_i - 50) \quad (1)$$

n is the total number of days in the hydrological year (September 1st to August 31st of the following year). The total number of snow days in the hydrological year is defined as the SCD; D_i is the percentage of snow cover (%) in a pixel ($0 \leq D_i \leq 100$); and H is the Heaviside function, which is equal to 0 (1) for negative (positive) arguments.

$$SED = D_1 + SCD_1' \quad (2)$$

SED is the day of year (DOY) of the last day of snow cover in a hydrological year. D_1 represents January 21th (Julian calendar). SCD_1' indicates the snow-covered days within the period from January 21th to August 31th (Li et al. 2020).

$$SOD = D_2 - SCD_2' \quad (3)$$

SOD is the DOY when the first day of snow cover occurs. D_2 represents January 20 (Julian calendar). This is the time when the snow in CTMR reaches its maximum. SCD_2' represents the number of snow days from September 1st to January 20th of the following year (Li et al. 2020).

3.2.2 Determination of vegetation phenology

The SOS, EOS and LOS were used to reflect the phenological changes in vegetation. The SOS, which is based on remote sensing technology, refers to the date when most plants in the community begin to expand leaves and grow normally. After this date, vegetation enters the rapid growth stage. The EOS refers to the date on which most of the plants in the community cannot grow normally and the leaves begin to turn yellow, after which the vegetation enters the stage of death or dormancy (Fu et al. 2018). The LOS is equal to the EOS minus the SOS, which is inconsistent with the traditional growth season concept of “the number of days a plant can grow in a year”. The remote sensing estimation results were based on the phenological status of vegetation in a community or region, and they presented a certain difference from traditional phenological results, although the correlation was very high (Zhang et al. 2003).

To remove the noise derived from cloud contamination in the time series, MOD13A1 images were first smoothed using the Savitzky–Golay (S-G) filtering method in TIMESAT software (Bian et al. 2009). Then, the dynamic threshold method was used to extract the vegetation phenology parameters

(Jonsson et al. 2002; Guang et al. 2019). This method is suitable for determining the vegetation phenology in large-scale areas (Ma et al. 2015):

$$N_{NDVI_{lim}} = (N_{NDVI_{max}} - N_{NDVI_{min}}) \times C \quad (4)$$

where $N_{NDVI_{lim}}$ is the dynamic threshold; $N_{NDVI_{max}}$ is the maximum value of the NDVI (normalized difference vegetation index); $N_{NDVI_{min}}$ is the minimum value of the rising (descending) stage of NDVI; and C is the coefficient.

The threshold coefficients of the SOS and EOS were set to 0.2 and 0.5, respectively. The two time points corresponding to the lowest values on both sides of the NDVI fitting curve peak were used to determine the critical phenological period. These two thresholds were verified in the field and have been used by most researchers (Mou et al. 2012; Huang et al. 2019; Fu et al. 2021).

3.2.3 Statistical analyses

The Pearson correlation coefficients between snow phenology and vegetation phenology were calculated to investigate the relationship between vegetation growth and snow (Wang et al. 2018). In addition, we performed a t -test to reflect the significance level (P value) of the relationship. This study examined the correlations in each pixel to identify spatial patterns. We selected the pixels with significant correlations ($P < 0.1$) to further investigate the relationships among different ecogeographical zones.

3.2.4 Grey relation analysis

Grey relational analysis (GRA) can be used in supplier selection decision-making for a large number of uncertain factors and their relationships, and it organically combines quantitative and qualitative methods, thereby clarifying and simplifying the original complicated problems. This method eliminates the subjective arbitrariness of decision-makers to a certain extent. To explain the response of vegetation phenology to snow phenology, this study used the GRA method to determine the grey relation grade (GRG) between the vegetation phenology and snow phenology parameters (Li et al. 2016; Chang et al. 2018; He et al. 2018). GRA establishes the degree of correlation between two corresponding sequences based on the similarity of the geometry of the comparison sequence and the reference sequence curve. The degree of correlation depends on the similarity of the two curves. In this study, snow

phenology parameters were defined as the comparison sequence $X_i=X_i(k)$ (where $i=1, 2, 3, 4, k=1, 2, \dots, n$). The vegetation phenology parameters were defined as the reference sequence X_o . The data were normalized to eliminate the effect of magnitude:

$$X'_i(k) = \frac{X_i(k) - \overline{X_i}}{\sigma_i} \quad (5)$$

$$X'_o(k) = \frac{X_o(k) - \overline{X_o}}{\sigma_o} \quad (6)$$

$\overline{X_i}$ and $\overline{X_o}$ are the comparison sequence and the reference sequence, respectively. σ_i and σ_o are defined as the standard deviations of the comparison sequence and the reference sequence, respectively.

$$\xi_{x_i}(k) = \frac{\Delta \min + \alpha \Delta \max}{\Delta \delta_i(t) + \alpha \Delta \max} \quad (7)$$

$\xi_{x_i}(k)$ denotes the grey correlation coefficient. $\Delta \delta_i(t)$ represents the absolute value of the difference between the $\overline{X_i}$ and the $\overline{X_o}$. $\Delta \min$ and $\Delta \max$ represents the minimum and maximum values of $\Delta \delta_i(t)$, respectively. α represents the resolution coefficient. The resolution was best when $\alpha \leq 0.5463$ (Zhang et al. 2018); therefore, α was set to 0.5 in this study.

The mean values of the grey correlation coefficients in the sequence were calculated to obtain the GRG values as follows:

$$r_i = \frac{\sum_{k=1}^n \xi_i(k)}{n} \quad (8)$$

$\xi_i(k)$ represents the grey correlation coefficient. r_i represents the GRG of the $\overline{X_i}$ and the $\overline{X_o}$.

4 Results

4.1 Distribution pattern of vegetation phenology

The spatial distribution of vegetation phenology and its standard deviation in the CTMR were calculated based on MOD13A1 NDVI data (Fig. 2). The spatial distribution of the mean SOS values varied significantly (Fig. 2a). The SOS showed a gradual delay from lower to higher elevations, which presented strong spatial heterogeneity. An early SOS occurred on the northern slope of the CTMR and the Yili Valley area (mostly on 0-82 DOY), accounting for 16.06% of the CTMR. The SOS occurred later in the middle part of the CTMR (mostly after 118 DOY),

accounting for 37.78% of the CTMR. The latest SOS occurred after 137 DOY. The EOS distribution was opposite to that of the SOS (Fig. 2c). The EOS generally occurred earlier at higher elevations and later at lower elevations. The EOS was late on the northwest slope of the CTMR and the Yili Valley (mostly occurring at 321-334 DOY), accounting for 30.18% of the study area. The EOS was the earliest in the middle part of the CTMR (92-298 DOY), accounting for 10.80% of the study area. The LOS showed a similar spatial pattern to the EOS and ranged from 24 d to 251 d (Fig. 2e). In this study, vegetation with a growing season less than 233 d was regarded as having a short LOS, and the opposite pattern indicated a long LOS. A long LOS was mainly distributed on the north slope, accounting for 69.50% of the study area, and a short LOS was mostly located in the middle part of the CTMR, accounting for 30.50% of the study area. The NDVI_{max} value of the western Yili Valley was the highest. The NDVI_{max} value of the Bayanbulak steppe in the central part was the second. On the whole, the distribution pattern of NDVI_{max} showed a high spatial heterogeneity (Fig. 2g). Because the western Yili Valley had a low elevation (500-780 m), superior natural conditions, abundant precipitation, a continental temperate climate, mild humid and fertile land. The surrounding mountain areas were dense, lush and grassy, so the NDVI_{max} value in this area was the highest. The interannual variation was smaller on the northern slope of the CTMR and the edge of the Yili Valley and ranged from 0-13 d. The interannual variation in the central ridgeline area was concentrated within 13-20 d. Strong variability was not observed in the spatial distribution of the standard deviation between the EOS and SOS, although a relatively smaller area showed lower interannual EOS variations (Fig. 2b, Fig. 2d)). The interannual variations in the LOS in most of the CTMR were in the range of 16-30 d (Fig. 2f). The larger interannual variations were mainly located in the Yili Valley of the CTMR, where the standard deviation exceeded 49 d. From the spatial distribution of NDVI_{max} standard deviation (Fig. 2h), the interannual fluctuation of NDVI_{max} in CTMR was relatively stable. The interannual fluctuation of NDVI_{max} in a large area ranged from 0 to 0.1, and only a few parts of the western Yili Valley were high (0.1-0.2). No significant differences in vegetation phenology were observed among the different ecogeographical zones (Fig. 3a). IID3 had the earliest SOS, the longest LOS,

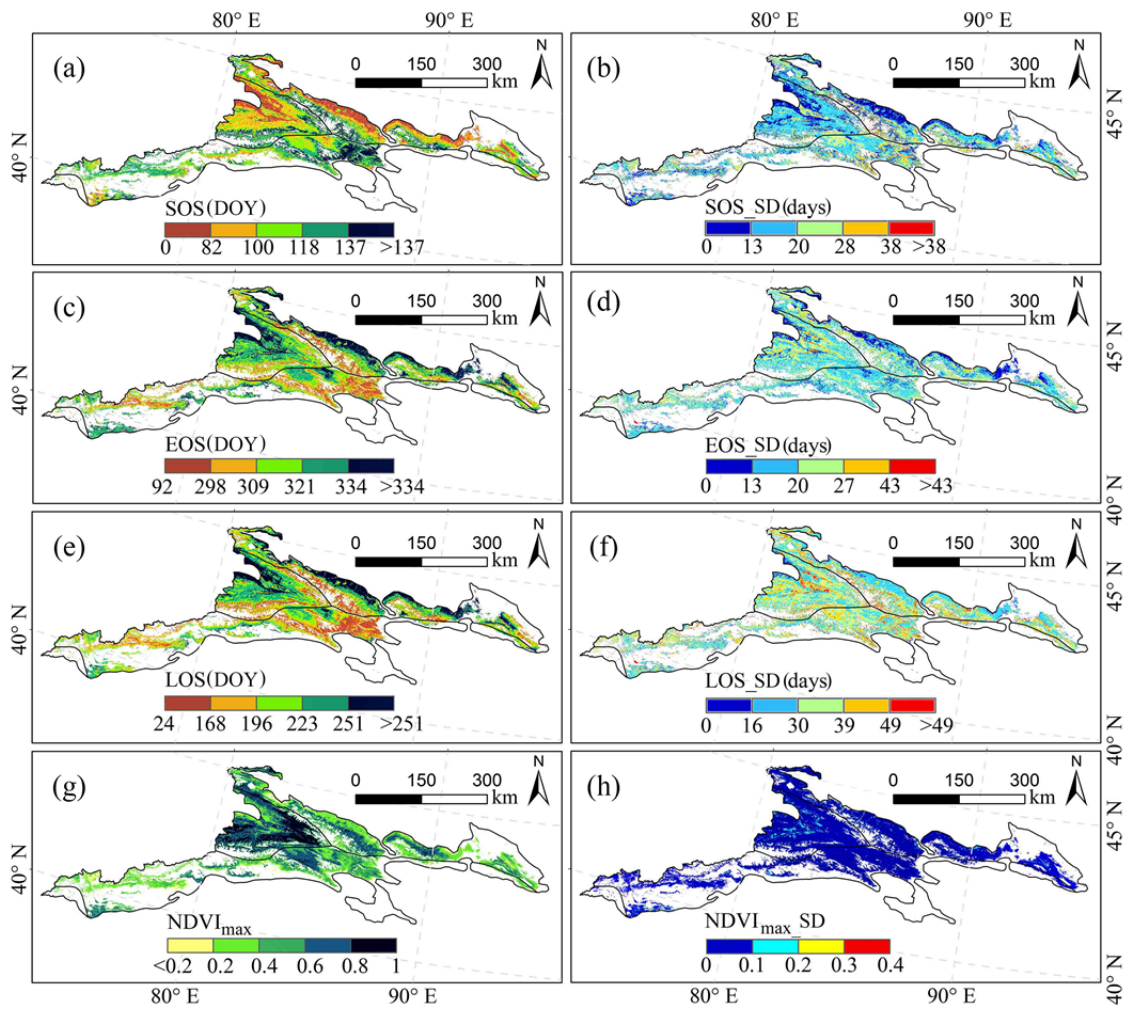


Fig. 2 Mean value and standard deviation of the start of growing season (SOS) (a and b, respectively), end of growing season (EOS) (c and d, respectively), length of growing season (LOS) (e and f, respectively) and $NDVI_{max}$ (g and h, respectively) from 2002 to 2018.

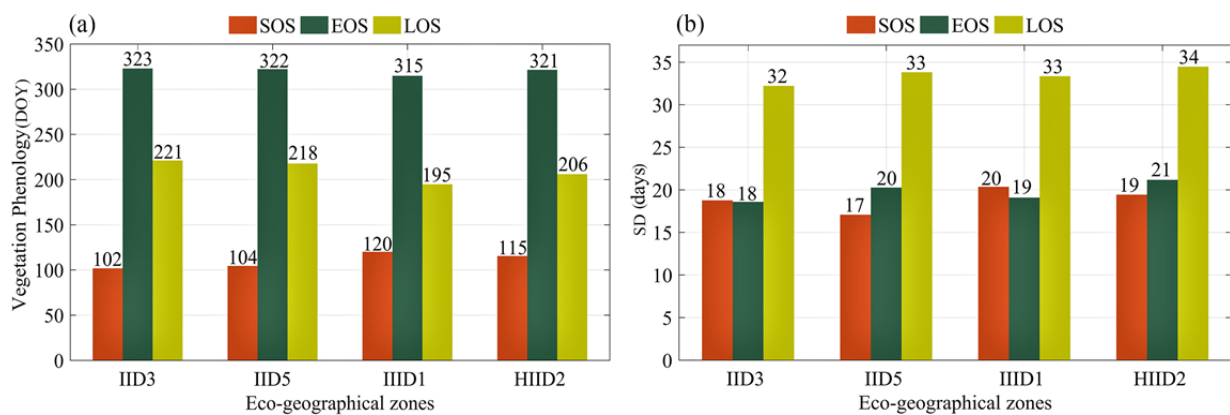


Fig. 3 Vegetation phenology (a) and standard deviation (SD) (b) in different eco-geographical zones.

and the latest EOS. From the standard deviation of vegetation phenology across the different eco-geographical zones, HIID2 exhibited an unstable state (Fig. 3b).

4.2 Distribution pattern of snow phenology

Based on the daily cloud-free snow data, the spatial distribution patterns of snow phenology and their standard deviation distributions were obtained

for 2002-2018 in the CTMR. Due to the heterogeneity of climate, topography and other factors, the snow distribution was not uniform and presented obvious geographical differences. Fig. 4a shows that the SOD occurred early in the central ridge region and late on the southern slope. The SOD generally occurred earlier at high elevations, with the earliest appearance in the ridge region (244-272 DOY), where high elevation and low temperature had favourable conditions for snowfall formation. The SOD was generally higher at lower elevations. The SOD in the northern and eastern parts of the CTMR mainly occurred from 344-364 DOY (December), while the SOD in the southern and southeastern areas mainly occurred from 364-21 (next year) DOY. Fig. 4c shows that the SED occurred later at higher elevations and earlier at lower elevations. The SED occurred earlier than 121 DOY in the large mountainous region, accounting for 75.77% of the total mountain area, and later than 121 DOY in the perennial snow and glacier-covered areas of the high-altitude mountains, accounting for 24.23% of the total mountain area. Along the mountain range, the SCD exhibited an overall pattern of high in the west and low in the east, high in the north and low in the south (Fig. 4e). High values (SCD > 269 d, approximately 9 months) were mainly located in the permanent snow and glacier-covered region of the high-altitude mountains, accounting for 3.17% of the total mountain area, and SCD values spanning 39-91 d were mainly distributed around the permanent snow area, the Yili Valley and the northern foothills of the CTMR. The SCD was less than 39 d in the valley of the CTMR and most of the middle- and low-elevation areas in the southern foothills, accounting for 52.76% of the total mountain area. This value was less than that of other areas and contributed more to spring snowmelt runoff. The interannual variations in the SOD were larger (28-49 d) along the middle ridge of the CTMR. The interannual variations in the SOD in the Bayanbulak steppes were 19-28 d, and the fluctuations in other regions were less than 19 d (Fig. 4b). The standard deviation of the SED (Fig. 4d) was similar to that of the SCD (Fig. 4f). It can be concluded that the interannual variations in the SED and SCD were large in the high-elevation perennially snow-covered and glacier-covered areas of the CTMR, with the SED fluctuating above 19 d and SCD fluctuating above 36 d. The interannual variations in the SED were 5-11 d in the Yili Valley area and below 5 d on the southern

slope. The snow phenology of different ecogeographical zones had obvious differences. IID5 had the latest SOD, the shortest SCD, and the earliest SED. IID1 had the earliest SOD, the longest SCD, and the latest SED (Fig. 5a). No major differences in snow phenology standard deviations were observed among the different ecogeographical zones (Fig. 5b).

4.3 Impact of snow phenology on vegetation phenology

4.3.1 SOS response to snow phenology

Fig. 6a shows that the SOD was positively correlated with the SOS in nearly 47.36% of the study area, of which 6.42% was significantly positively correlated ($P < 0.1$), mainly in the Yili Valley, the Bayanbulak steppe area, and the southwest slope (Fig. 6b), which meant that the SOS would be advanced with an earlier SOD. The correlation analysis also showed that the SED and SOS were positively correlated in nearly 36.34% of the study area (Fig. 6c), with 6.43% of the area showing a significant ($P < 0.1$) positive correlation (Fig. 6d) and most of the Yili Valley and part of the Bayanbulak steppes (63.66%) showing a negative correlation, thus implying that the SOS in this area would advance with a delayed SED. A total of 54.78% of the study areas showed a negative correlation between the SCD and SOS (Fig. 6e), with 9.58% of the areas presenting a significant ($P < 0.1$) negative correlation (Fig. 6f), mainly in the Yili Valley, Bayanbulak Steppes and the southwest slope. This finding indicates that the SOS in the following year would advance because of the longer SCD. Nearly 45.22% of the study area showed a positive correlation between the SCD and SOS. A high SCD may also contribute to the delayed SOS.

The SCD and SED were negatively correlated with the SOS in all four ecogeographic zones (Table 2). The SCD had the strongest negative correlation with the SOS of IID5 (middle temperate zone). The SED had the strongest negative correlation with the SOS of IID1 (warm temperate zone). The SOD was positively correlated with the SOS of IID3 (mid-temperate zone) and IID1 and negatively correlated with the SOS of IID5 and IID2. This result indicated that the SOS advanced with increases in the SCD and delays in the SED in all four ecogeographic zones. Advancement of the SOD may advance the SOS of IID3 (mid-temperate zone) and IID1. In addition, a delay of the SOD may advance the SOS of IID5 (mid-

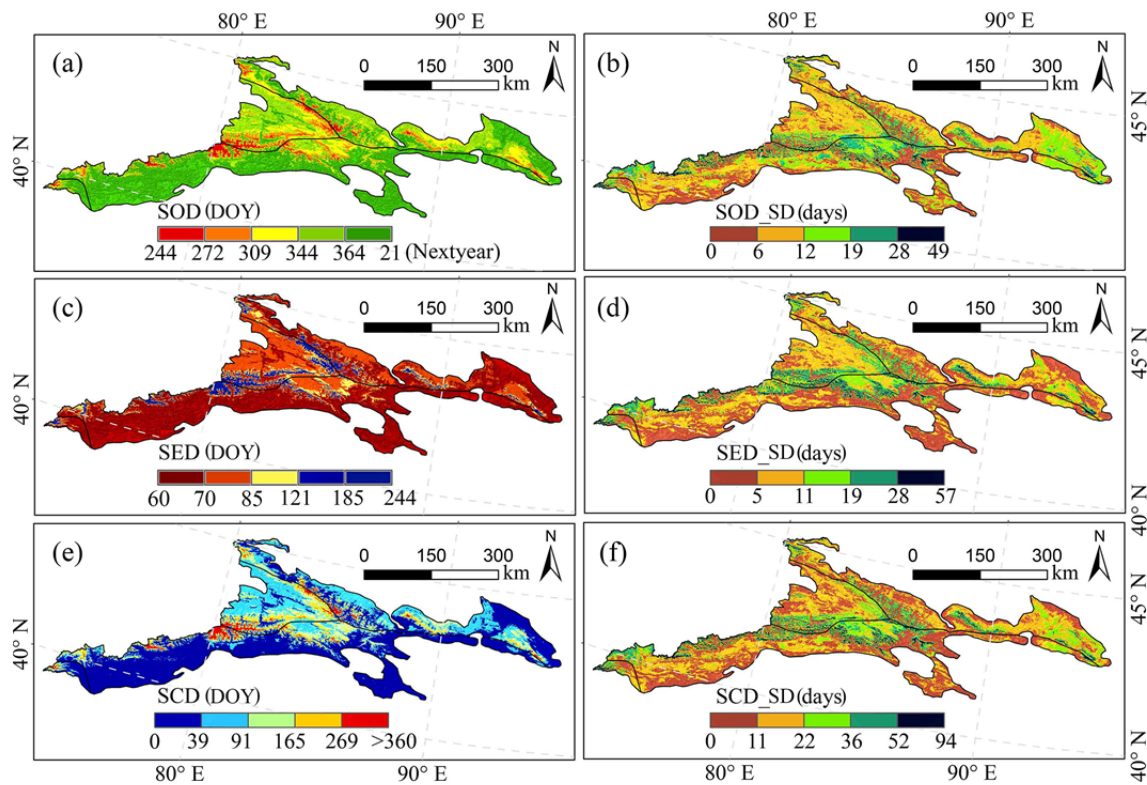


Fig. 4 Mean value and standard deviation of the snow onset date (SOD) (a and b, respectively), snow end date (c and d, respectively) and snow cover days (SCD) (e and f, respectively) from 2002 to 2018.

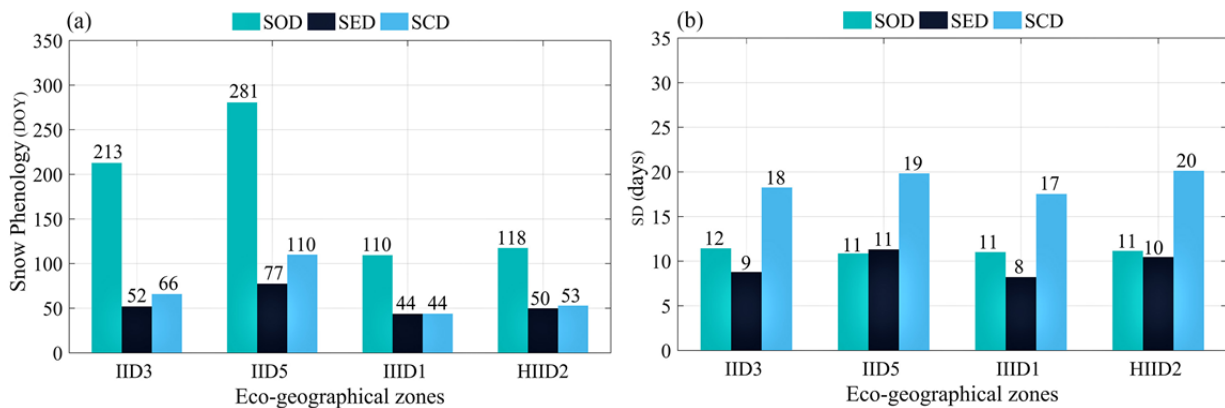


Fig. 5 Snow phenology (a) and standard deviation (SD) (b) in different eco-geographical zones.

temperate zone) and HIID2 (highland temperate zone).

4.3.2 LOS response to snow phenology

Snow cover also affected the LOS. The spatial distribution of the correlation between snow cover and the LOS was also spatially heterogeneous, with 46.67% of the study area presenting a negative correlation between the SOD and LOS (Fig. 7a), among which 5.81% was significantly negatively correlated ($P < 0.1$), mainly in the Yili Valley, southwest slope, northeast slope and southeast slope

(Fig. 7b). This finding indicates that a delay in the SOD would contribute to a shortening of the LOS. In other areas, the SOD was positively correlated with the LOS. A total of 66.85% of the CTMR showed a positive correlation between the SED and LOS (Fig. 7c), among which 15.74% was significantly ($P < 0.1$) positively correlated, mainly in the northwestern part of the CTMR (the Yili Valley) and the southwestern slope (Fig. 7d). This finding implies that an increase in the SCD would contribute to an increase in the LOS. A negative correlation was observed between the SED and LOS in a small part of the central region and

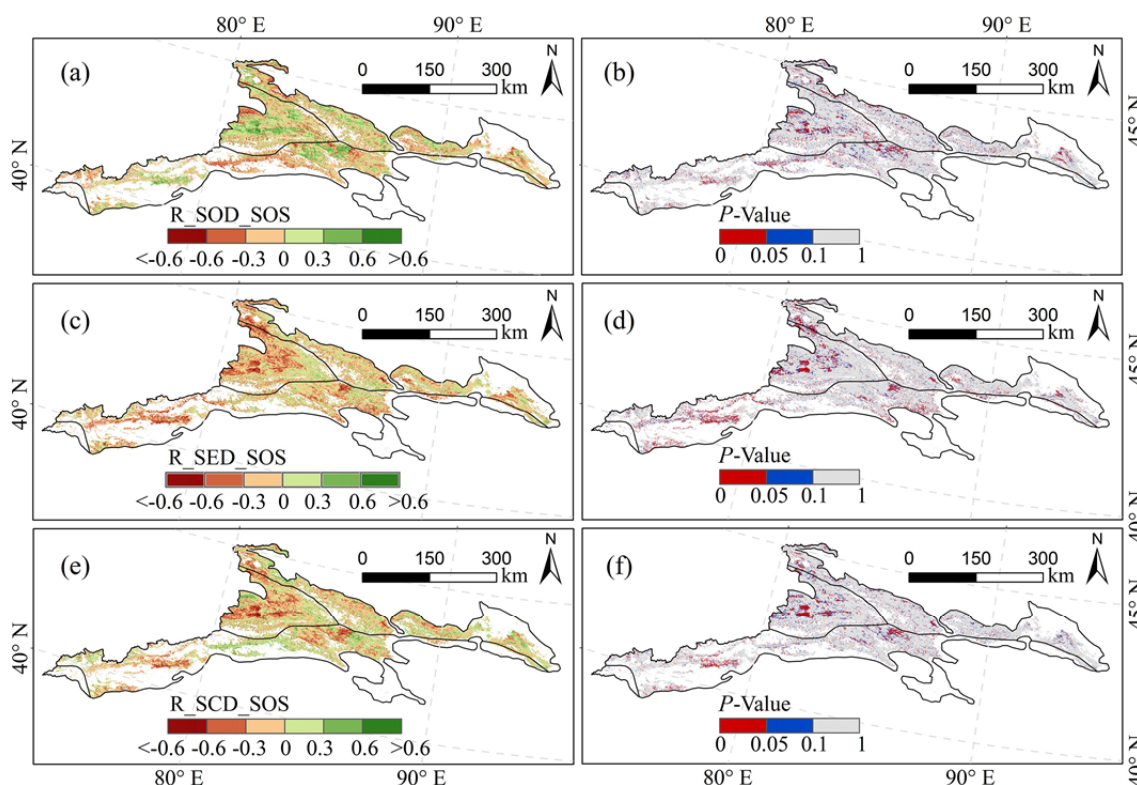


Fig. 6 Spatial patterns of the correlation coefficient between the start of growing season (SOS) and snow phenology: (a) correlation coefficient between the snow onset date (SOD) and SOS and (b) *P* value; (c) correlation coefficient between snow end date (SED) and SOS and (d) *P* value; and (e) correlation coefficient between SCD and SOS and (f) *P* value.

Table 2 Pearson correlation coefficients between the start of growing season (SOS) and the snow phenology parameters of the four ecogeographical zones in the Chinese Tianshan mountainous region

Ecogeographical zone	SCD		SOD		SED	
	<i>R</i>	Count	<i>R</i>	Count	<i>R</i>	Count
IID3	-0.25**	12025	0.15**	14784	-0.39**	14720
IID5	-0.44**	17878	-0.26**	15162	-0.45**	17754
IIID1	-0.31**	19472	0.20**	19398	-0.50**	26933
HIID2	-0.15*	103	-0.19**	109	-0.41**	146

Notes: * $P < 0.1$; ** $P < 0.05$.

part of the southern slope (33.15%). The SCD and LOS were positively correlated in nearly 44.10% of the study area (Fig. 7e), with a total of 10.35% of the area significantly ($P < 0.1$) positively correlated, mainly in the Yili Valley and southwestern slopes of the CTMR (Fig. 7f). This indicates that a large amount of snow cover would contribute to an increase in the LOS. However, only a small portion of the area (4.12%) showed a significant negative correlation, and it was distributed in the ridgeline region, meaning that an increase in the SCD would contribute to a shortening of the LOS.

The SCD and SED were positively correlated with the LOS in all four ecogeographical zones (Table 3) and showed the strongest positive correlation with the

LOS of IID5. The SOD was negatively correlated with the SOS of IID3 and IIID1 but positively correlated with the SOS of IID5 and HIID2. This finding indicated that the LOS increased in all four ecogeographic zones with increases in the SCD and delays in the SED. A delay in the SOD can advance the SOS of IID3 and IIID1 and delay the SOS of IID5 and HIID2.

4.3.3 EOS response to snow phenology

The relation between snow phenology and the EOS was spatially heterogeneous. A total of 69.55% of the study area showed a negative correlation between the SOD and EOS (Fig. 8a), among which 11.65% was significantly negatively correlated ($P < 0.1$), indicating

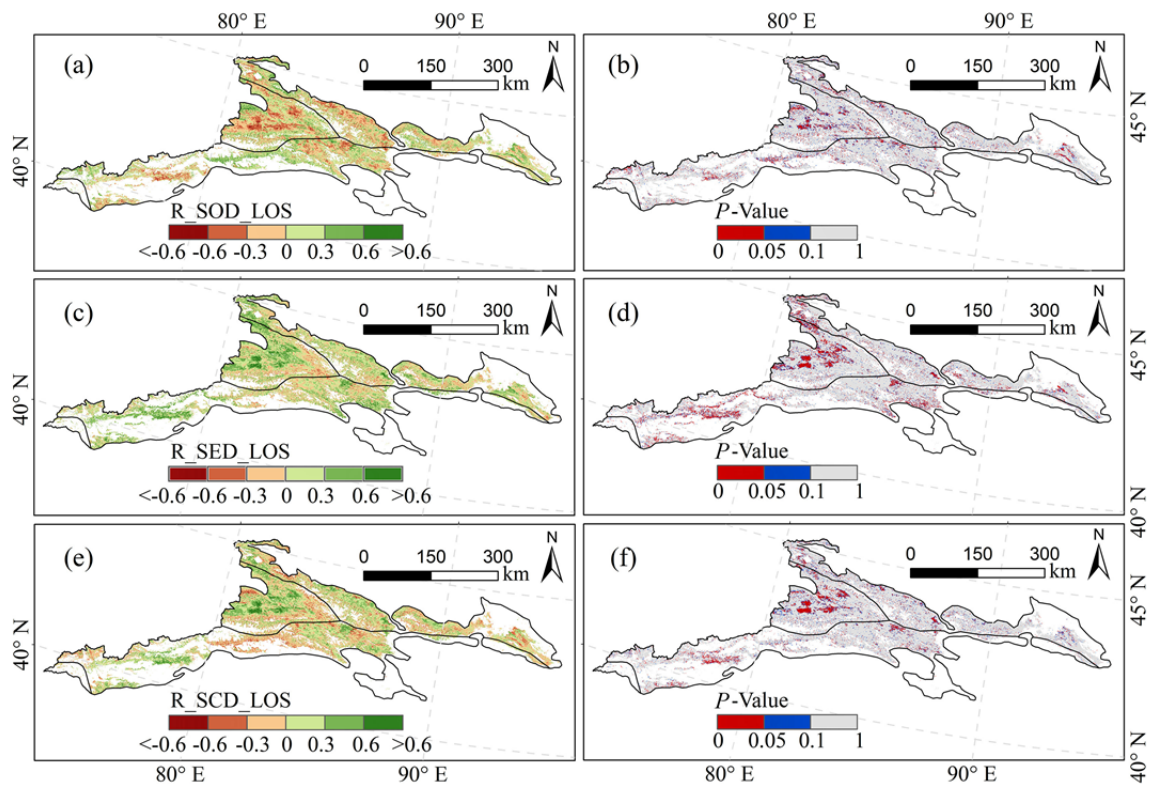


Fig. 7 Spatial patterns of the correlation coefficient between the length of growing season (LOS) and snow phenology: (a) correlation coefficient between SOD and LOS and (b) *P* value; (c) correlation coefficient between SED and LOS and (d) *P* value; and (e) correlation coefficient between SCD and LOS and (f) *P* value.

Table 3 Pearson correlation coefficients between the length of growing season and the snow phenology parameters of the four ecogeographical zones in the Chinese Tianshan mountainous region

Ecogeographical zone	SCD		SOD		SED	
	<i>R</i>	Count	<i>R</i>	Count	<i>R</i>	Count
IID3	0.26**	12947	-0.16**	14631	0.42**	16810
IID5	0.40**	21995	0.36**	15717	0.53**	24337
IIID1	0.33**	18089	-0.14**	17734	0.47**	27822
HIID2	0.12*	100	0.29**	109	0.42**	131

Notes: * $P < 0.1$; ** $P < 0.05$

that an advanced SOD could delay the EOS in the following year. This study also observed a significant positive ($P < 0.1$) relationship in a small area (7.39%) of the southwestern slope (Fig. 8b), which meant that an advanced SOD corresponded to an advanced EOS. A total of 43.05% of the study area showed a negative correlation between the SED and EOS (Fig. 8c), among which 7.52% was significantly negatively correlated ($P < 0.1$) in the Yili Valley. A small area (11.03%) exhibited a significantly positive relationship on the southwestern slope (Fig. 8d). An advanced SED would delay the EOS in the Yili Valley but advance the EOS on the southwest slope. A total of 66.99% of the study area showed a positive correlation between the SCD and EOS (Fig. 8e), among which 11.92% were significantly positively

correlated ($P < 0.1$) in the Yili Valley. Nevertheless, a small area (4.31%) exhibited a significantly negative relationship on the southwestern slope (Fig. 8f). A longer SCD would delay the EOS in the Yili Valley and advance the EOS on the southwest slope.

As shown in Table 4, the SED was positively correlated with the EOS of all four ecogeographic zones. The SED was most closely correlated with the EOS of IIID1. The SCD was positively correlated with the EOS of IID3, IID5 and IIID1 and was negatively correlated with the EOS of HIID2 and EOS. The SOD was positively correlated with EOS of IID3, HIID2 and IID5 and negatively correlated with the EOS in IIID1. This finding indicated that the EOS of all four ecogeographic zones advanced with the advancement of the SED. An increase in the SCD would delay the

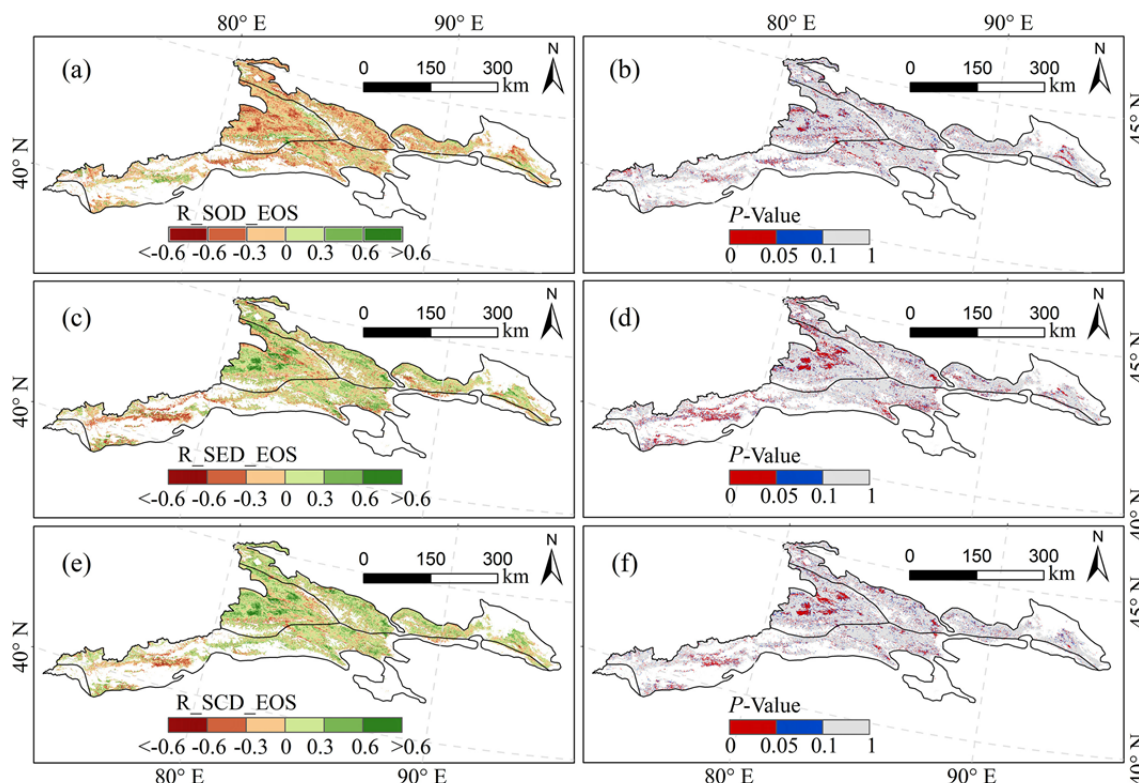


Fig. 8 Spatial patterns of the correlation coefficient between the EOS and snow phenology: (a) correlation coefficient between SOD and EOS and (b) *P* value; (c) correlation coefficient between SED and EOS and (d) *P* value; (e) correlation coefficient between SCD and EOS and (f) *P* value.

Table 4 Pearson correlation coefficients between the end of growing season and the snow phenology parameters of the four ecogeographical zones in the Chinese Tianshan mountainous region

Ecogeographical zone	SCD		SOD		SED	
	<i>R</i>	Count	<i>R</i>	Count	<i>R</i>	Count
IID3	0.33**	15400	0.35**	15994	0.36**	18682
IID5	0.41**	23798	0.42**	17896	0.35**	26096
IIID1	0.34**	21141	-0.14**	21010	0.52**	30894
HIID2	-0.04	92	0.07	119	0.25**	132

Notes: * $P < 0.1$; ** $P < 0.05$.

EOS of IID3, IID5 and IIID1 and advance the EOS of HIID2. A delay in the SOD contributes to a delay of the EOS of IID3, IID5 and HIID2 and an advancement in the EOS in IIID1.

4.4 Response of vegetation phenology to snow phenology

The responses of the vegetation phenology of four typical alpine vegetation types to snow phenology in the CTMR were examined separately based on the grey correlation analysis method. The GRG values reflect the degree of influence of different snow phenology parameters on alpine vegetation phenology parameters. Fig. 9a shows that for the four vegetation types, the mean GRG of the SOD reached the

maximum values (0.6955, 0.7103, 0.7668, and 0.6916), while the mean GRG of the SCD reached the minimum values (0.6220, 0.6524, 0.6494, and 0.5770). The degree of influence of snow phenology parameters on the SOS varied among the vegetation types. The vegetation SOS was most strongly influenced by the SOD, followed by the SED, with the SCD having the weakest influence. Fig. 9b shows that the vegetation EOS was most strongly influenced by the SED, followed by the SOD, with the SCD having the weakest effect on the EOS in the alpine meadows and sparse shrubs. In alpine meadows and alpine sparse vegetation, the vegetation EOS was most strongly influenced by the SOD, followed by the SED, with the SCD having the weakest effect. The SOS in the four alpine vegetation cover types was most

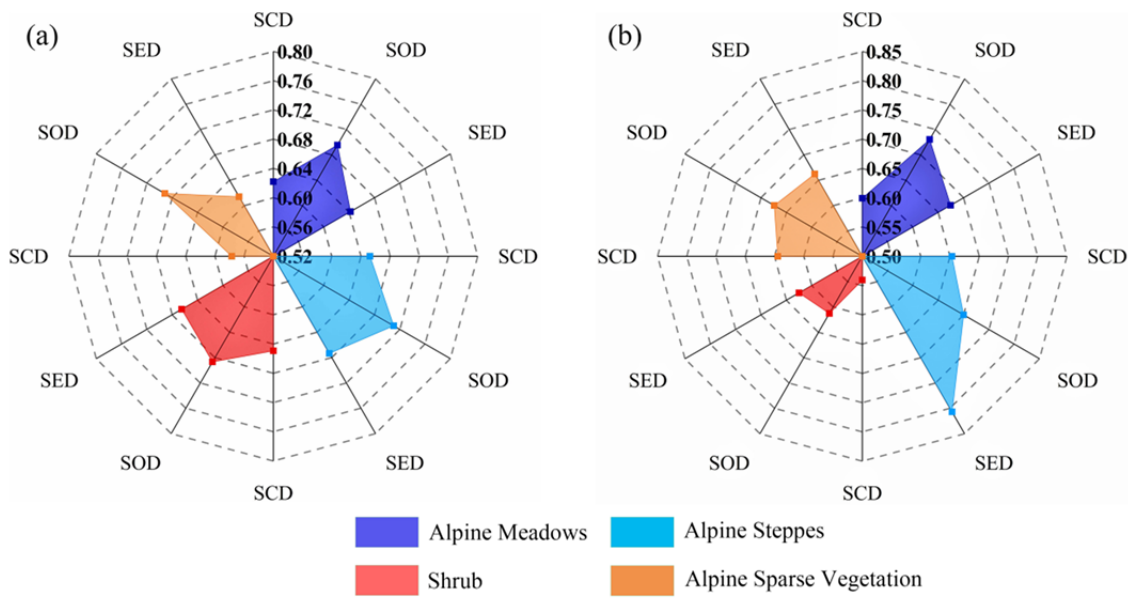


Fig. 9 Grey relation grade (a) between the SOS and the snow phenology parameters) and (b) between the EOS and the snow phenology parameters for the different vegetation types in the Chinese Tianshan mountainous region. SOD: Snow onset date, SED: snow end date, SCD: snow cover days.

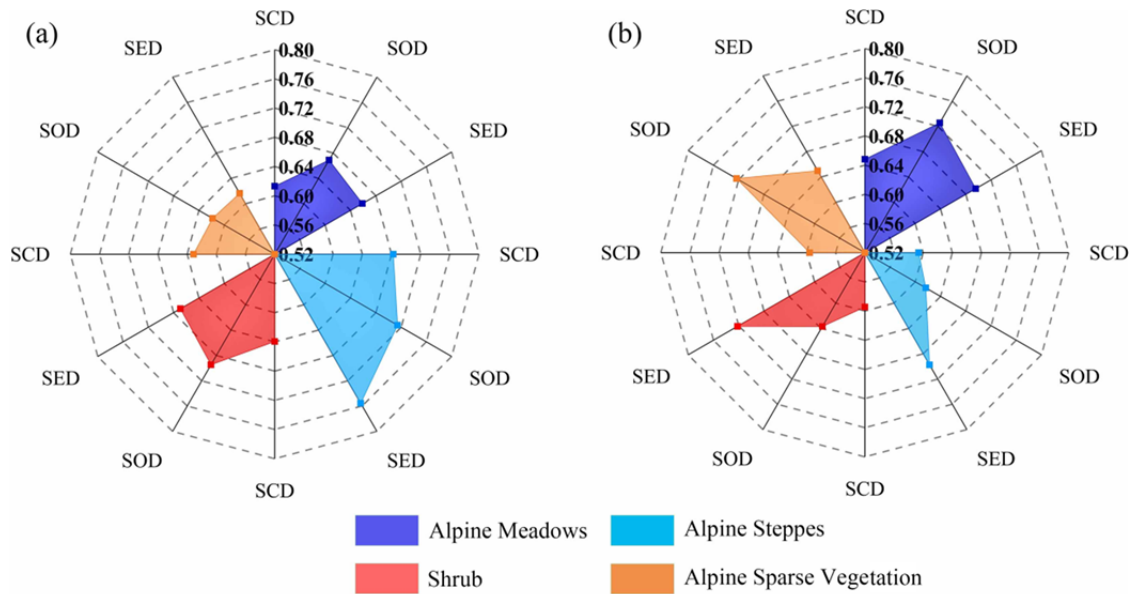


Fig. 10 Grey relation grade (a) between the LOS and the snow phenology parameters and (b) between the NDVI_{max} and the snow phenology parameters for different vegetation types in the Chinese Tianshan mountainous region. SOD: Snow onset date, SED: snow end date, SCD: snow cover days.

strongly affected by the SOD, followed by the SED, with the SCD having the weakest effect. The effect of the SOD on the EOS was greatest in alpine meadows and sparse alpine vegetation. The evaluation of the impact of snow phenology parameters on the EOS showed that different vegetation cover types presented various orders. The SED had the largest impact on the EOS in alpine steppes and shrubs, while the SCD had the smallest impact.

Fig. 10a shows the effect of the snow phenology parameters on the LOS in different vegetation types. For the alpine meadows and shrubs, the LOS was most strongly affected by the SOD, followed by the SED and SCD. For the alpine steppes, the LOS was most strongly affected by the SED, followed by the SOD and SCD. For the alpine sparse vegetation, the order of effect was opposite to that of the alpine steppes, with the LOS most strongly affected by the

SCD, followed by the SOD and SED. Fig. 10b shows the effects of the snow phenology parameters on the $NDVI_{max}$ in different vegetation types. For the alpine meadows and shrubs, the effect of snow phenology parameters on $NDVI_{max}$ showed the same order, with SED having the strongest effect, followed by the SOD and SCD. For the alpine meadows and sparse alpine vegetation, the SOD had the greatest effect, followed by the SED and SCD.

5 Discussion

5.1 Influence of snow phenology on vegetation phenology

The northern regions showed a higher SCD, earlier SOD, and later SED than the southern regions. Because the south slopes were sunny, they received more solar radiation energy. Additionally, due to being exposed to cold northerly and northwesterly air inflows, the south-facing and northwestern slopes receive far less precipitation than the northern slopes, which are moistened by the North Atlantic air circulation (Li et al. 2020). Relatively sufficient water resources can promote the growth of vegetation, resulting in a late EOS (Dilixiati et al. 2019); therefore, the EOS occurred later in areas with relatively good hydrothermal conditions (northwest slope of the CTMR and the Yili Valley). We found that the SCD was positively correlated with the SOS but negatively correlated with the LOS in most parts of the CTMR. These results agreed with previous studies showing that a higher SCD in winter delays the SOS and reduces the LOS (Jonas et al. 2008; Xie et al. 2017; Wang et al. 2018b). However, we found the different effects of the SCD on the SOS and LOS in the Yili Valley and the Bayanbulak, implying that a long-term SCD would also advance the SOS and increase the LOS in the following year. Overall, long-term snow cover time leads to the higher snow depth, which can increase the amount of water available to plants in subsequent growing seasons (Peng et al. 2010). Snow is also an effective insulator, protecting the soil from the harsh climatic conditions (low temperatures and strong winds) of CTMR (Yu et al. 2013). As a result, soil temperatures in snow-covered areas were generally higher than in snow-free areas (Freppaz et al. 2008). It was also beneficial to the SOS. Most of the SED in the CTMR occurred between

the end of February and mid-April (Li et al. 2020), and most vegetation started to grow after late March. Therefore, a close relationship between snow phenology and the SOS can be suggested. Earlier snowmelt may expose the soil to freezing events and reduce soil moisture, as shown in a long-term field experiment in a woodland in the northeastern region of the United States (Groffman et al. 2001). Despite favourable temperature conditions, vegetation will not be able to obtain sufficient moisture from snow if the SED is too early, which explains the negative correlation between the SED and SOS in warm areas (Yili Valley). A similar situation was observed for the LOS. The earlier SED delayed the SOS and thus reduced the LOS in relatively dry areas.

5.2 Responses among different vegetation types

The response of vegetation growth to snow cover dynamics varies greatly among different vegetation types in the high latitudes of the Northern Hemisphere (Eugster et al. 2010). We found that the effect of SED on LOS, EOS and $NDVI_{max}$ in alpine steppes was more obvious than that of other vegetation types. This may be because shorter plants growing on grasslands are more likely to be completely covered with snow than taller plant types. Therefore, long-term snow cover can help grasslands resist low temperatures effectively. In addition, alpine steppes were mainly distributed in arid or semi-arid areas. The snow cover may have an important impact on soil moisture in this area. On the premise of keeping soil temperature stable, snow cover can delay the change of soil moisture and promote the increase of soil moisture. This can promote the growth of alpine steppes. The change of snow cover in winter may also affect the nutrients needed for vegetation growth and the length of vegetation growth cycle by changing the hydrothermal conditions of the soil (Wang et al. 2018b). The SOD had the greatest influence on the SOS, EOS, LOS and $NDVI_{max}$ of alpine meadow vegetation. Alpine meadows were mainly distributed in the middle of CTMR, where the temperature was low, but the soil moisture was good. The SOD can indirectly reflect the temperature and precipitation of CTMR in autumn and winter. For example, the early appearance of SOD will lead to frostbite on the surface of vegetation, which will cause serious damage to vegetation and affect the

development of vegetation in the follow year (Sa et al. 2021). The vegetation phenology of different vegetation types in the CTMR can be attributed to the different water-heat combinations in different ecological environments and other factors. The hydrothermal combination was restricted by latitude, longitude, topography and human activities (Fu et al. 2021). In future studies, the snow cover dynamics and vegetation growth dynamics should be comprehensively monitored to clarify the mechanism of snow phenology impacts on vegetation growth in the CTMR.

6 Conclusion

In this study, the spatial and temporal patterns of snow phenology and vegetation phenology in the CTMR were analysed based on daily cloud-free snow data and MOD13A1 data from 2002-2018. The effects of snow phenology change on vegetation phenology were studied using correlation analysis and GRA analysis methods. The conclusions are outlined as follows.

(1) The SOD was earlier at higher elevations and later at lower elevations in the CTMR. The SED and SOD exhibited opposite spatial distributions. Snow was widely distributed in the CTMR. The high-value area of SCD (>269 d) was mainly distributed in the middle part of the CTMR and the ridgeline area, while the low-value area (<39 d) was concentrated on the southern slope and northeastern edge of the CTMR. The SCD presented an overall pattern of high in the west and low in the east, high in the north and low in the south, roughly spreading over the mountain range direction.

(2) The spatial distribution of the SOS in the CTMR was characterized by a gradual delay from lower to higher elevations with strong spatial

heterogeneity. The EOS was late on the northwest slope of the CTMR and the Yili Valley. The earliest EOS was distributed in the middle part of the mountain. The LOS exhibited a similar spatial pattern as the EOS. The long LOS was mainly distributed in the northern slope and the Yili Valley, while the short LOS was mainly located in the middle part of the CTMR.

(3) The correlation between vegetation phenology and snow phenology in different ecogeographic zones was diverse. The effect of snow phenology on vegetation phenology was more distinct in IID5 (Yili Valley) than in the other ecogeographic zones. A negative correlation was observed between the SOS and SED in most areas, and a positive correlation was observed between the LOS and SED. The sensitivity of vegetation phenology to changes in snow phenology varied among the different vegetation types. The SOD had the greatest effect on the SOS. In contrast, the SCD had the weakest impact on the SOS. The SED had the greatest influence on the EOS in alpine steppes and shrubs.

Acknowledgements

This research was supported by the National Natural Science Foundation of China (41761014), the “One Hundred Outstanding Young Talents Training Program” of Lanzhou Jiaotong University, the National Natural Science Foundation of China (41971094) and the Youth Innovation Promotion Association CAS (2019414). We thank the National Glacial Permafrost and Desert Data Centre, National Qinghai-Tibet Plateau Scientific Data Centre, Scientific Data Centre of Cold and Arid Regions of the Chinese Academy of Sciences and Resource and Environmental Science Data Centre of the Chinese Academy of Sciences for data support.

References

- Ahmed A, Nawaz R, Woulds C, et al. (2020) Influence of hydro-climatic factors on future coastal land susceptibility to erosion in Bangladesh: a geospatial modelling approach. *JGSA* 4(1): 6. <https://doi.org/10.1007/s41651-020-00050-x>
- Bian JH, Li AN, Song MQ, et al. (2010) Reconstruction of MODIS vegetation index time series by Savitzky-Golay filtering algorithm. *J Remote Sens* 14(4): 725-741. (In Chinese)
- Buus-Hinkler J, Hansen BU, Tamstorf MP, et al. (2006) Snow-vegetation relations in a high Arctic ecosystem: Inter-annual variability inferred from new monitoring and modeling concepts. *Remote Sens Environ* 105(3): 237-247. <https://doi.org/10.1016/j.rse.2006.06.016>
- Chang S, Huang F, Zhao JJ, et al. (2018) Identifying influential climate factors of land surface phenology changes in Songnen Plain of China using grid-based grey relational analysis. *J Grey Syst-Uk* 30(4): 18-33.
- Chen X, An S, Inouye DW, et al. (2015a) Temperature and snowfall trigger alpine vegetation green-up on the world's roof. *Global Change Bio* 21(10): 3635-3646. <https://doi.org/10.1111/gcb.12954>

- Chen X, Liang S, Cao Y, et al. (2015b) Observed contrast changes in snow phenology in northern middle and high latitudes from 2001–2014. *Sci Rep-UK* 5(1): 16820. <https://doi.org/10.1038/srep16820>
- Desai AR, Wohlfahrt G, Zeeman MJ, et al. (2016) Montane ecosystem productivity responds more to global circulation patterns than climatic trends. *Environ Res Lett* 11(2): 13-24. <https://doi.org/10.1088/1748-9326/11/2/024013>
- Dilixiati M, Rusuli Y, Namaiti H, et al. (2019) The phenological characteristics and climatic response of vegetation in the Xinjiang Tianshan Mountains, China. *Clim Chang Res* 15 (6): 624-632. (In Chinese)
- Ding YX, Peng SZ (2020) Spatiotemporal trends and attribution of drought across china from 1901–2100. *Sustainability-Basel* 12(2): 477. <https://doi.org/10.3390/su12020477>
- Dorji T, Totland Ø, Moe SR, et al. (2013) Plant functional traits mediate reproductive phenology and success in response to experimental warming and snow addition in Tibet. *Global Change Bio* 19(2): 459–472. <https://doi.org/10.1111/gcb.12059>
- Eugster W, Rouse WR, Sr R, et al. (2010) Land–atmosphere energy exchange in Arctic tundra and boreal forest: available data and feedbacks to climate. *Global Change Bio* 6(S1): 84-115. <https://doi.org/10.1046/j.1365-2486.2000.06015.x>
- Freppaz M, Celi L, Marchelli M, et al. (2010) Snow removal and its influence on temperature and N dynamics in alpine soils (Vallée d'Aoste, northwest Italy). *J Plant Nutr Soil Sc* 171(5): 672-680. <https://doi.org/10.1002/jpln.200700278>
- Frick A, Tervooren S (2019) A framework for the long-term monitoring of urban green volume based on multi-temporal and multi-sensoral remote sensing data. *JGSA* 3(1): 6. <https://doi.org/10.1007/s41651-019-0030-5>
- Fu Y, Chen H, Niu HH, et al. (2018) Spatial and temporal variation of vegetation phenology and its response to climate changes in Qaidam Basin from 2000 to 2015. *J Geogr Sci* 28(4): 400-414. <https://doi.org/10.1007/s11442-018-1480-2>
- Fu Y, Chen H, Zhang S (2021) Phenological characteristics of cold and arid regions based on community types and their response to climatic factors-- A case study of Qaidam Basin from 2000 to 2019. *Geogr Res* 40 (1): 52-66. (In Chinese)
- Groffman PM, Driscoll CT, Fahey TJ, et al. (2001) Colder soils in a warmer world: A snow manipulation study in a northern hardwood forest ecosystem. *Biogeochemistry* 56(2): 135-150. <https://doi.org/10.2307/1469925>
- Guan QH, Ding MJ, Zhang HM (2019) Spatial-temporal variation of spring phenology and its response to climate change in alpine grassland in Qinghai-Tibet Region. *M Res* 37(05): 639-648. (In Chinese)
- He D, Yi GH, Zhang TB, et al. (2018) Temporal and spatial characteristics of EVI and its response to climatic factors in recent 16 years based on grey relational analysis in Inner Mongolia Autonomous Region, China. *Remote Sens-Basel* 10(6): 961. <https://doi.org/10.3390/rs10060961>
- Hu RJ (2004) China Tianshan Natural Geography. China Environmental Publishing House, Beijing. (In Chinese)
- Huang WL, Zhang Q, Kong DD, et al. (2019) Response of vegetation phenology to drought in Inner Mongolia from 1982 to 2013. *Act Eco Sin* 39(13): 4953-4965. (In Chinese)
- Ide R, Oguma H (2013) A cost-effective monitoring method using digital time-lapse cameras for detecting temporal and spatial variations of snowmelt and vegetation phenology in alpine ecosystems. *Ecol Inform* 16: 25-34. <https://doi.org/10.1016/j.ecoinf.2013.04.003>
- Inouye DW (2008) Effects of climate change on phenology, frost damage, and floral abundance of montane wildflowers. *Ecology* 89(2): 353-362. <https://doi.org/10.1890/06-2128.1>
- Jin HX, Jönsson AM, Bolmgren K, et al. (2017) Disentangling remotely-sensed plant phenology and snow seasonality at northern Europe using MODIS and the plant phenology index. *Remote Sens Environ* 198: 203–212. <https://doi.org/10.1016/j.rse.2017.06.015>
- Jonas T, Rixen C, Sturm M, et al. (2008) How alpine plant growth is linked to snow cover and climate variability. *J Geophys Res* 113(G3). <https://doi.org/10.1029/2007jg000680>
- Jonsson P, Ekkhund L (2002) Seasonality extraction by function fitting to time-series of satellite sensor data. *Ieee T Geosci Remote* 40(8): 1824-1832. https://doi.org/10.1142/9789812796752_0022
- Julitta T, Cremonese E, Migliavacca M, et al. (2014) Using digital camera images to analyse snowmelt and phenology of a subalpine grassland. *Agr Forest Meteorol* 198: 116-125. <https://doi.org/10.1016/j.agrformet.2014.08.007>
- Justice C, Vermote E, Townshend J (1998) The moderate resolution imaging spectroradiometer (MODIS): land remote sensing for global change research. *Ieee T Geosci Remote* 36(4): 1228-1249. <https://doi.org/10.1109/36.701075>
- Körner C (2005) The green cover of mountains in a changing environment. In: Huber UM, Bugmann HKM, Reasoner MA (eds.), *Global Change and Mountain Regions*. Springer. pp 367-375.
- Li HD, Li YK, Gao YY, et al. (2016) Human impact on vegetation dynamics around Lhasa, southern Tibetan Plateau, China. *Sustainability-Basel* 8(11): 1146. <https://doi.org/10.3390/su8111146>
- Li LH, Li XM, Zhang FY, et al. (2018) The study of snow in Tianshan Mountains, North west China. China Agricultural Publishing Press. (In Chinese)
- Li XM, Gao P, Li Q, Tang H, et al. (2016) Multipath analysis of response of Tianshan snow cover to climate change in China. *Clim Chang Res* 12 (4): 303-312. (In Chinese)
- Li YP, Chen YN, Li Z (2019) Developing daily cloud free snow composite products from MODIS and IMS for the Tianshan Mountains. *Earth Space Sci* 6(2): 266-275. <https://doi.org/10.1029/2018EA000460>
- Li YP, Chen YN, Li Z, et al. (2020) Climate and topographic controls on snow phenology dynamics in the Tianshan Mountains, Central Asia. *Atmos Res* 236: 140813. <https://doi.org/10.1016/j.atmosres.2019.104813>
- Liu J, Zhang W, Liu T (2017) Monitoring recent changes in snow cover in Central Asia using improved MODIS snow-cover products. *J. Arid Land* 9: 763–777. <https://doi.org/10.1007/s40333-017-0103-6>
- Liu Z, Wu C, Liu Y, et al. (2017) Spring green-up date derived from GIMMS3g and SPOT-VGT NDVI of winter wheat cropland in the North China Plain. *Isprs J Photogramm* 130:81-91. <https://doi.org/10.1016/j.isprsjprs.2017.05.015>
- Ma XP, Bai HY, He YN, et al. (2015) The Vegetation Remote Sensing Phenology of Qinling Mountains Based on NDVI and its Response to Temperature: taking within the territory of shaanxi as an example. *Sci Geo Sinica* 35(12): 1616-1621. (In Chinese)
- Miao G, Shi LP, Nan C et al. (2015) Precipitation impacts on vegetation spring phenology on the Tibetan Plateau. *Glob Chang Biol* 21(10): 3647-3656. <https://doi.org/10.1111/gcb.12961>
- Mou MJ, Zhu WQ, Wang LG, et al. (2012) Evaluation of remote sensing extraction methods for vegetation phenology based on flux tower net ecosystem carbon exchange data. *Chinese J Applied Eco* 23(2): 319-327. (In Chinese)
- Ozanne C, Anhuif D, Boulter S, et al. (2003) Biodiversity Meets the Atmosphere: A Global View of Forest Canopies. *Science* 301(5630): 183-186. <https://doi.org/10.1126/science.1084507>
- Paudel K P, Anders en P (2013) Response of rangeland vegetation to snow cover dynamics in Nepal Trans Himalaya. *Climatic Change* 117: 149-162.

- <https://doi.org/10.1007/s10584-012-0562-x>
Peng SZ, Ding YX, Liu W, et al. (2019) 1 km monthly temperature and precipitation dataset for China from 1901 to 2017. *Earth System Science Data* 11(4): 1931–1946.
<https://doi.org/10.5194/essd-11-1931-2019>
- Peng SZ, Ding YX, Wen ZM, et al. (2017) Spatiotemporal change and trend analysis of potential evapotranspiration over the Loess Plateau of China during 2011–2100. *Agr Forest Meteorol* 233(Complete): 183–194.
<https://doi.org/10.1016/j.agrformet.2016.11.129>
- Peng SZ, Gang C, Cao Y, et al. (2018) Assessment of climate change trends over the Loess Plateau in China from 1901 to 2100. *Int J Climatol* 38(5): 2250–2264.
<https://doi.org/10.1002/joc.5331>
- Peng, S (2019) 1-km monthly mean temperature dataset for China (1901-2017). National Tibetan Plateau Data Center.
<https://10.11888/Meteorol.tpcd.270961.CSTR:18406.11>
- Peng, S (2020) 1-km monthly precipitation dataset for China (1901-2017). National Tibetan Plateau Data Center.
<https://doi.org/10.5281/zenodo.3185722>
- Qiu YB, Wang XX (2020) 2002-2018 High Asia daily snow coverage data set. National Cryosphere Desert Data Center (www.ncdc.ac.cn).
<https://doi:10.11922/sciencedb.45>
- Richardson AD, Keenan TF, Migliavacca M, et al. (2013) Climate change, phenology, and phenological control of vegetation feedbacks to the climate system. *Agr Forest Meteorol* 169(3): 156–173.
<https://doi.org/10.1016/j.agrformet.2012.09.012>
- Sa CL, Meng FB, Luo M, et al. (2021) Spatiotemporal variation in snow cover and its effects on grassland phenology on the Mongolian Plateau. *J Arid Land* 13(3): 332–349.
<https://doi.org/10.1007/s40333-021-0056-7>
- Shen MG, Tang YH, Chen J, et al. (2011) Influences of temperature and precipitation before the growing season on spring phenology in grasslands of the central and eastern Qinghai-Tibetan Plateau. *Agr Forest Meteorol* 151(12): 1711–1722.
<https://doi.org/10.1016/j.agrformet.2011.07.003>
- Tang ZG, Wang XR, Jian W, et al. (2017) Spatiotemporal variation of snow cover in the CTMR Mountainous, Central Asia, based on cloud-free modis fractional snow cover product, 2001–2015. *Remote Sens-Basel* 9(10): 1045.
<https://doi.org/10.3390/rs9101045>
- Thomey ML, Collins SL, Vargas R, et al. (2011) Effect of precipitation variability on net primary production and soil respiration in a Chihuahuan Desert grassland. *Global Change Bio* 17(4): 1505–1515.
<https://doi.org/10.1111/j.1365-2486.2010.02363.x>
- Thompson JA, Paull DJ, Lees BG (2015) Using phase-spaces to characterize land surface phenology in a seasonally snow-covered landscape. *Remote Sens of Environ* 166:178–190.
<https://doi.org/10.1016/j.rse.2015.04.008>
- Vitasse Y, Rebetez M, Filippa G, et al. (2017) 'Hearing' alpine plants growing after snowmelt: ultrasonic snow sensors provide long-term series of alpine plant phenology. *Int J of Biometeorol* 61(2): 349–361.
<https://doi.org/10.1007/s00484-016-1216-x>
- Wang K, Zhang L, Qiu YB, et al. (2015) Snow effects on alpine vegetation in the Qinghai-Tibetan Plateau. *Int J Digit Earth* 8(1): 58–75.
<https://doi.org/10.1080/17538947.2013.848946>
- Wang S, Wang X, Chen G, et al. (2017) Complex responses of spring alpine vegetation phenology to snow cover dynamics over the Tibetan Plateau, China. *Sci Total Environ* 593–594: 449–461.
<https://doi.org/10.1016/j.scitotenv.2017.03.187>
- Wang S, Zhang B, Yang Q, et al. (2017) Responses of net primary productivity to phenological dynamics in the Tibetan Plateau, China. *Agr Forest Meteorol* 232(Complete): 235–246.
<https://doi.org/10.1016/j.agrformet.2016.08.020>
- Wang T, Peng S, Lin X, et al. (2013) Declining snow cover may affect spring phenological trend on the Tibetan Plateau. *P Natl Acad Sci U S A* 110(31): E2854–E2855.
<https://doi.org/10.1073/pnas.1306157110>
- Wang X, Xie H (2009) New methods for studying the spatiotemporal variation of snow cover based on combination products of MODIS Terra and Aqua. *J Hydrol* 371(1–4): 192–200.
<https://doi.org/10.1016/j.jhydrol.2009.03.028>
- Wang XY, Wang SY, Hang Y, et al. (2016) Snow phenology variability in the Qinghai-Tibetan Plateau and its response to climate change during 2002–2012. *J Geo-Infor Sci* 18(11): 1573–1579. (In Chinese)
- Wang XY, Wu CY, Peng DL, et al. (2018b) Snow phenology affects alpine vegetation growth dynamics on the Tibetan Plateau: Satellite observed evidence, impacts of different biomes, and climate drivers. *Agr Forest Meteorol* 256: 61–74.
<https://doi.org/10.1016/j.agrformet.2018.03.004>
- Wang YC, Sun YL, Wang ZL (2014) Spatial-temporal change in vegetation cover and climate factor drivers of variation in the haihe River Basin 1998–2011. *Resour Sci* 36(3): 594–602. (In Chinese)
- Wu CY, Hou XH, Peng DL, et al. (2016) Land surface phenology of China's temperate ecosystems over 1999–2013: Spatial-temporal patterns, interaction effects, covariation with climate and implications for productivity. *Agr Forest Meteorol* 216: 177–187.
<https://doi.org/10.1016/j.agrformet.2015.10.015>
- Xie J, M Kneubühler, Garonna I, et al. (2017) Altitude-dependent influence of snow cover on alpine land surface phenology. *J Geophys Res-Bioge* 122(5): 1107–1122.
<https://doi.org/10.1002/2016JG003728>
- Yu H, Luedeling E, Xu J (2010) Winter and spring warming result in delayed spring phenology on the Tibetan Plateau. *P Natl A Sci India B* 107(51): 22151–22156. <https://doi.org/10.1073/pnas.1012490107>
- Yu Z, Liu SR, Wang JX, et al. (2013) Effects of seasonal snow on the growing season of temperate vegetation in China. *Glob. Change Biol* 19(7) 2182–2195.
<https://doi.org/10.1111/gcb.12206>
- Zhang JB, Deng ZF (1987) *Precipitation of Xinjiang*. Meteorology Press. (In Chinese)
- Zhang QY (2018) Study on the response of grass yield to winter snow cover in Hulunbuir grassland based on RS and GIS. Master Thesis, Shandong Normal University. (In Chinese)
- Zhang XY, Friedl MA, Schaaf CB, et al. (2003) Monitoring vegetation phenology using MODIS. *Remote Sens Environ* 84(3): 471–475.
[https://doi.org/10.1016/S0034-4257\(02\)00135-9](https://doi.org/10.1016/S0034-4257(02)00135-9)
- Zhang Y, Wang G, Wang Y, et al. (2010) Response of biomass spatial pattern of alpine vegetation to climate change in permafrost region of the Qinghai-Tibet Plateau, China. *J Mt Sci* 7(4): 301–314.
<https://doi.org/10.1007/s11629-010-2011-5>